NRC Research Press

ARTICLE

Performance of manned and unmanned aerial surveys to collect visual data and imagery for estimating arctic cetacean density and associated uncertainty[1]

M.C. Ferguson, R.P. Angliss, A. Kennedy, B. Lynch, A. Willoughby, V. Helker, A.A. Brower, and J.T. Clarke

Abstract: Manned aerial surveys have been used successfully for decades to collect data to infer cetacean distribution, density (number of whales/km^2), and abundance. Unmanned aircraft systems (UAS) have potential to augment or replace some manned aerial surveys for cetaceans. We conducted a three-way comparison among visual observations made by marine mammal observers aboard a Turbo Commander aircraft; imagery autonomously collected by a Nikon D810 camera system mounted to a belly port on the Turbo Commander; and imagery collected by a similar camera system on a remotely controlled ScanEagle® UAS operated by the US Navy. Bowhead whale density estimates derived from the marine mammal observer data were higher than those from the Turbo Commander imagery; comparisons to the UAS imagery depended on survey sector and analytical method. Beluga density estimates derived from either dataset collected aboard the Turbo Commander were higher than estimates derived from the UAS imagery. Uncertainties in density estimates derived from the marine mammal observer data were lower than estimates derived from either imagery dataset due to the small sample sizes in the imagery. The visual line-transect aerial survey conducted by marine mammal observers aboard the Turbo Commander was 68.5% of the cost of the photo strip-transect survey aboard the same aircraft and 9.4% of the cost of the UAS survey.

Key words: UAS, bowhead whale, gray whale, beluga, Beaufort Sea, Chukchi Sea.

Résumé : Les levés réalisés au moyen d'aéronefs pilotés ont été utilisés avec succès pendant des décennies pour recueillir des données afin de déduire la répartition, la densité (nombre de baleines/km^2) et l'abondance des cétacés. Les systèmes d'aéronef sans pilote (UAS) pourraient compléter ou remplacer certains levés aériens avec pilote sur les cétacés. Nous avons effectué

Received 3 January 2018. Accepted 5 May 2018.

M.C. Ferguson and R.P. Angliss. Marine Mammal Laboratory, Alaska Fisheries Science Center, NOAA, National Marine Fisheries Service, Seattle, WA 98115, USA.
A. Kennedy, A. Willoughby, and A.A. Brower. Marine Mammal Laboratory, Alaska Fisheries Science Center, NOAA, National Marine Fisheries Service, Seattle, WA 98115, USA; Joint Institute for the Study of the Atmosphere and Ocean, University of Washington, Seattle, WA 98195, USA.
B. Lynch. Center for Coastal Studies, Provincetown, MA 02657, USA.
V. Helker. Lynker Technologies, LLC, Leesburg, VA 20175, USA.
J.T. Clarke. Leidos, Arlington, VA 22203, USA.
Corresponding author: Megan Ferguson (e-mail: megan.ferguson@noaa.gov).
[1]This paper is one of two companion papers published in this issue of J. Unmanned Veh. Syst. (Angliss et al. 2018. J. Unmanned Veh. Syst. This issue. dx.doi.org/10.1139/juvs-2018-0001).

une comparaison entre trois types de levés, soit des observations visuelles de mammifères marins faites par des chercheurs à bord d'un aéronef Turbo Commander ; des images recueillies de façon autonome par un système photographique Nikon D810 monté dans un hublot sous le Turbo Commander; et des images recueillies par un système photographique semblable sur un UAS ScanEagle® télécommandé utilisé par les Forces navales des États-Unis. Les estimations de densité de baleines boréales provenant des données des observateurs de mammifères marins étaient plus élevées que celles des images à partir du Turbo Commander; les comparaisons avec l'imagerie UAS variaient selon le secteur du levé et la méthode analytique. Les estimations de densité de bélugas provenant de l'un ou l'autre des ensembles de données recueillies à bord du Turbo Commander étaient plus élevées que les estimations provenant de l'imagerie UAS. Les incertitudes au niveau des estimations de densité provenant des données des observateurs de mammifères marins étaient inférieures aux estimations provenant de l'un ou l'autre des ensembles de données d'imagerie en raison des petites tailles des échantillons au niveau de l'imagerie. Le levé aérien par transect effectué visuellement par des observateurs à bord du Turbo était 68,5 % du coût du levé par transect de bande de photos à bord du même aéronef et 9,4 % du coût du levé UAS. [Traduit par la Rédaction]

Mots-clés : système d'aéronef sans pilote (UAS), baleine boréale, baleine grise, béluga, mer de Beaufort, mer des Tchouktches.

Introduction

In recent years, there has been increasing interest in understanding the degree to which unmanned aircraft systems (UAS) could be used to augment or replace manned aerial surveys for studying cetaceans. A UAS comprises an aircraft without a human pilot onboard, a ground- or ship-based controller (pilot), and the communication system connecting the aircraft to the pilot. The aircraft is referred to as an unmanned aerial vehicle (UAV). If successful, using UAS to address questions in marine mammal ecology and management may decrease risk to personnel, increase survey efficiency, and minimize disturbance to wildlife.

In general, to further our understanding of cetacean ecology, the following questions are representative of what needs to be answered. How many individuals of each species or population are found in a given area and time period, and how does that density (number of animals per unit area) vary on time scales spanning hours to decades? Are the animals distributed as large groups, small groups, or single individuals? Where and when do the animals feed, migrate, and reproduce? Is the species or population segregated by age or sex? The data required to address these questions are also required to address conservation and management issues relevant to management agencies and to entities, such as the military and industry, who are required to obtain authorization from management agencies to conduct certain activities in the marine environment. Furthermore, the issues of human safety, animal disturbance, project cost, efficiency, precision, and accuracy are common to both the scientific and management realms.

Manned aerial surveys from fixed-wing aircraft can efficiently and quickly survey large or remote areas, and have been used successfully for decades to achieve diverse scientific and wildlife management goals. In some cases, animal visibility is better from an aircraft than from a vessel or land. Additionally, due to the increased survey speed relative to marine mammals, aerial survey platforms reduce or eliminate potential biases in abundance or density estimates arising from animal movement (Buckland et al. 2001). Aerial line-transect surveys for marine mammals (Garner et al. 1999; Buckland et al. 2001) collect data that can be used to infer distribution, estimate density or abundance, and investigate habitat use and behavior. The National Oceanic and Atmospheric Administration (NOAA), Bureau of Ocean Energy Management (BOEM), US Navy (hereinafter referred to as Navy), petroleum industry, and others have relied on manned aerial line-transect surveys to collect large-scale information

on cetaceans for stock assessment purposes (e.g., Muto et al. 2017) and to evaluate the impacts of specific human activities on cetaceans (e.g., Clarke et al. 2017*b*).

There are numerous examples of the successful application of manned aerial surveys to study marine mammals in the Arctic. The Aerial Surveys of Arctic Marine Mammals (ASAMM) project, funded and co-managed by BOEM and conducted and co-managed by NOAA Fisheries, is one of the longest-term surveys for marine mammals in the world (Clarke et al. 2017*b*), with annual line-transect surveys dating back to 1979. Multiple federal and state agencies, academic institutions, and private companies rely on data in the ASAMM historical database to make decisions regarding marine mammal conservation and management, and to better understand marine mammal roles in the arctic ecosystem. In addition, aerial survey methods have been used successfully off Point Barrow, Alaska, to collect photo-identification data to estimate the abundance of the Western Arctic bowhead whale stock (Schweder 2003; Koski et al. 2010; Schweder et al. 2010; Mocklin et al. 2012*a*; Vate Brattström et al. 2016). Numerous studies of bowhead whale feeding behavior in the Alaska Arctic, specifically in the Barrow Canyon area (Mocklin et al. 2012*b*) and in the eastern Alaska Beaufort Sea (Richardson and Thomson 2002), have been conducted from aircraft. Furthermore, aerial surveys have been used regularly to mitigate and monitor the effects of anthropogenic activities, such as petroleum exploration operations (e.g., Richardson et al. 1985, 1986, 1987; Schick and Urban 2000).

Although decades of valuable research, monitoring, and mitigation activities have been successfully conducted from manned aircraft, these survey platforms have some specific limitations. First, observer discomfort or fatigue caused by extended periods of time aboard the aircraft can affect data collection. Second, there are risks inherent in manned aerial operations that must be mitigated to reach an acceptable level of safety for the survey team. Third, manned aircraft have the potential to disturb wildlife. Lastly, manned aircraft burn fuel at a relatively high rate, resulting in high costs and consumption of non-renewable resources.

UAS have only recently been used to study ecology and inform wildlife management, but their use is growing rapidly (e.g., Watts et al. 2010; Sarda-Palomera et al. 2012; Anderson and Gaston 2013; Vermeulen et al. 2013; Barasona et al. 2014; Chabot et al. 2015; Mulero-Pázmány et al. 2015; Vas et al. 2015; Rümmler et al. 2016), including marine mammal research applications. Hodgson et al. (2013) conducted within line-of-sight strip-transect surveys with a ScanEagle® to collect observations of dugongs (*Dugong dugon*), and Maire et al. (2013) initiated attempts to automate analysis of the resulting images. UAS are also used to survey pinnipeds. UAS have been successfully used to collect images of spotted (*Phoca largha*) and ribbon (*Phoca fasciata*) seals in the Bering Sea pack ice (Moreland et al. 2015), to survey leopard seals (*Hydrurga leptonyx*) and Antarctic fur seals (*Arctocephalus gazella*) in Antarctica (Goebel et al. 2015), and to collect images to assess abundance and pup production of Steller sea lions (*Eumetopias jubatus*) in the western Aleutian Islands (Fritz 2012; Sweeney et al. 2016). Koski et al. (2015) evaluated the use of UAS in the Canadian Arctic to collect high-resolution photographs to identify individual bowhead whales and they monitored the whales' observed reactions to UAS overflights.

The performance of existing UAS technology and sensors versus human observers in manned aircraft for collecting data on cetaceans across broad study areas is unknown but must be understood prior to using UAS to augment or replace manned aircraft surveys. In late summer 2015, BOEM, the Navy, and NOAA, in collaboration with Shell Oil and the North Slope Borough Department of Wildlife Management, conducted field operations in the northeastern Chukchi Sea and western Beaufort Sea. The objectives were to evaluate the ability of UAS technology (i.e., platforms, payloads, sensors, and software) to collect data to detect cetaceans, identify individuals to species, estimate group size, and identify calves relative to conventional aerial line-transect surveys by human observers and digital

photographic surveys conducted from fixed-wing manned aircraft. The target species were gray whales, bowhead whales, and belugas. All three species are protected under the US Marine Mammal Protection Act, the bowhead whale is granted additional protection as an endangered species under the US Endangered Species Act, and bowhead whales and belugas are of substantial interest and concern because they are hunted for subsistence. We estimated cetacean density and abundance in the survey area, and associated uncertainties in those estimates, and compared those values across all three datasets. Additionally, we compared the following performance metrics across datasets: number of sightings; ability to identify sightings to species; relative efficiency of each platform, measured by length of trackline and area covered, and the duration of survey and analytical effort required to achieve a pre-specified level of precision in the density estimate; and survey and analytical costs in both dollars and fuel consumption. Here, we provide recommendations for the types of cetacean study objectives that can likely be met by UAS currently and in the near future. Operational results and recommendations are described in a companion paper by Angliss et al. (2018).

Methods

Study area and survey timing

The study area encompasses approximately 16 800 km^2 of the northeastern Chukchi and western Beaufort seas (Fig. 1) (Angliss et al. 2018). Pre-determined transect lines, spaced 4.75 km apart, were located west (24 transects) and east (26 transects) of Point Barrow. The study area was partitioned into west (5140 km^2) and east (6149 km^2) sectors due to logistical (Angliss et al. 2018) and ecological considerations. Field operations occurred in 2015, beginning with the arrival of the UAS equipment aboard a Navy C130 aircraft on 19 August and ending with the last flight of the manned aircraft in the study area on 7 September (Angliss et al. 2018). The project was conducted during the time of year with documented peak cetacean abundance and weather conditions most conducive to flight operations in the study area.

The survey area provides important feeding grounds and migration pathways for gray whales, bowhead whales, and belugas, which use the area seasonally (e.g., Citta et al. 2015; Clarke et al. 2015, 2016, 2018; Stafford et al. 2016; Brower et al. 2017*b*). Gray whales are reliably found in high densities in the west sector during the open water (ice-free) season, which occurs from July to October. In some years, bowhead whales and belugas are found in high densities in the east sector, especially in the vicinity of Barrow Canyon. Known high-density areas were targeted to obtain the number of sightings required to derive robust analytical conclusions about the relative performance of manned aircraft and UAS in a reasonably short period. A sighting was defined as either a group (i.e., cluster) of closely associated animals, typically located within five body lengths of each other, or a single individual detected alone.

Field methods

UAS aerial surveys

Here, we provide a summary of our 2015 field methods. A more comprehensive and detailed description of field methods and aviation safety protocols for the UAS is provided in Angliss et al. (2018).

The ScanEagle® UAS was selected for this project based on its strong airworthiness history, relatively large payload capacity, and long endurance (24 h). A Nikon D810 high-resolution digital camera with 20-mm Nikkor f 2.8 lens, capable under ideal conditions of providing a minimum photographic ground resolution of 7 cm/pixel and minimum photographic strip width of 400–600 m at survey altitude, was directly exposed to the outside air. We expected this resolution would be sufficient for detecting individual large whales,

Fig. 1. Study area for the manned and unmanned aerial surveys of cetaceans conducted in late summer 2015. Transects shown were flown by both the manned and unmanned aircraft.

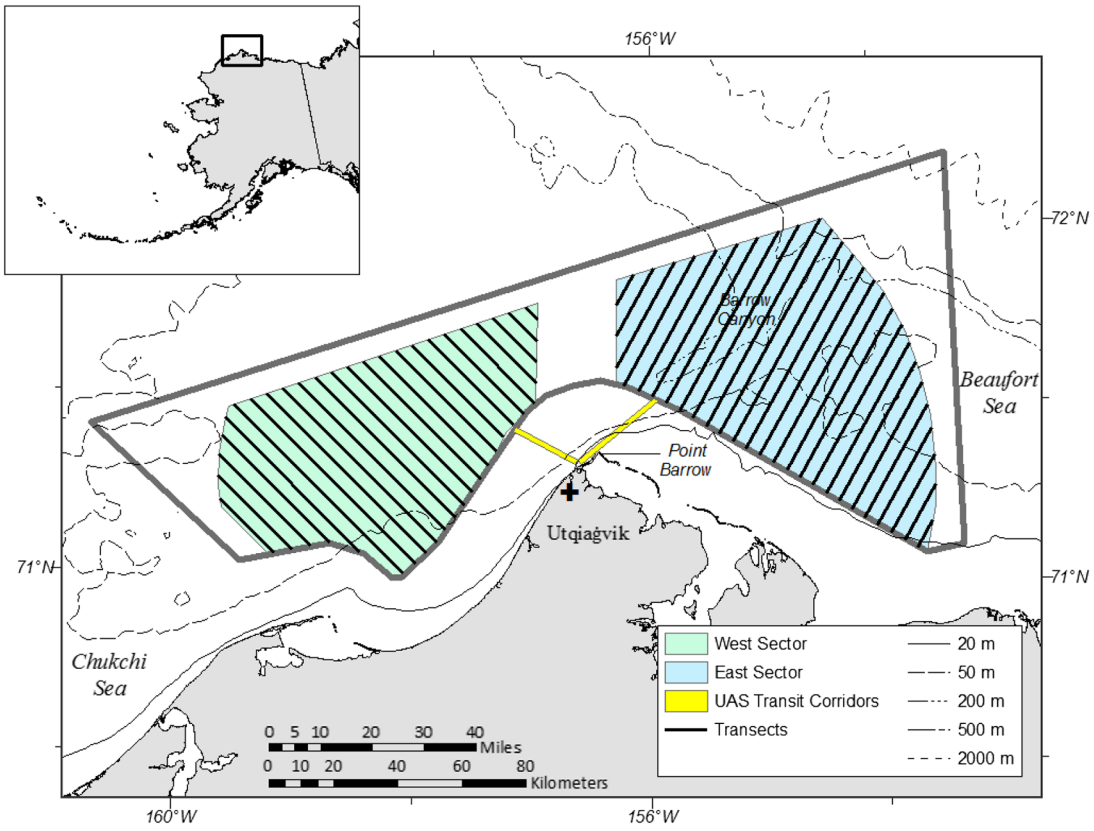

identifying animals to species, estimating group size, and determining whether calves were present. A global positioning system (GPS) pinger allowed position metadata to be simultaneously recorded with the images taken by the D810. Metadata automatically recorded for each image included latitude, longitude, and altitude. A camera trigger automatically collected photographs at pre-set distance intervals throughout the duration of each flight, based on position data from the GPS.

In a typical UAS flight, the UAV was launched and recovered from the shore-based station and accessed the offshore study area located in international airspace through one of two transit corridors (Fig. 1). The UAV remained at or below 122 m above mean sea level (AMSL) while inside the corridor to increase vertical separation with typical nearshore air traffic. Once in the offshore study area, the UAV increased altitude to the target altitude of 305 m AMSL and flew pre-programmed fine-scale (4.75 km apart) transects (Fig. 1) at 93–111 km/h, collecting high-resolution digital photographic strip-transect data every 100 m distance. Therefore, a given parcel of water on the surface of the ocean was visible in at least three consecutive images from the UAV. Occasionally, the UAV operated at lower altitudes, as necessary, to remain below the cloud bases. Transects were flown in passing mode, wherein the aircraft did not divert from the transect line or circle to investigate sightings. Once UAS operations were complete on a particular day, the UAV descended below 121 m AMSL while still in international airspace in the offshore study area and entered the transit corridor inbound for recovery at the shore-based station.

Aerial Surveys of Arctic Marine Mammals

ASAMM manned aerial line-transect surveys have been conducted annually in the western Beaufort Sea since 1979. Survey protocols have remained essentially constant since 1982 (Clarke et al. 2017*a*). These surveys were conducted from 1 July to 31 October 2015 over a larger expanse of the eastern Chukchi and western Beaufort seas (67°–72° latitude, −140° to −169° longitude, encompassing 240 000 km^2; Clarke et al. 2017*a*). In 2015, flight protocols were altered between 26 August and 7 September to follow the fine-scale transects in the UAS survey area (Fig. 1) and to provide a comparison between the UAS and manned aircraft surveys. Comprehensive and detailed field methods for the ASAMM project in 2015 are provided in Clarke et al. (2017*a*).

ASAMM marine mammal observers collected visual line-transect data on marine mammals and relevant environmental conditions from a fixed-wing, twin engine Turbo Commander aircraft flown by two pilots from Clearwater Air, Inc. ASAMM visual survey protocols followed standard line-transect procedures (Buckland et al. 2001). Crew positions and responsibilities, and recording of environmental, effort, and sighting data were identical to that described in Clarke et al. (2017*a*). The ASAMM aircraft surveyed at approximately 213 km/h at a target altitude of 320 m. All ASAMM surveys conducted in the UAS study area during the UAS field season implemented passing mode protocols to be consistent with the UAS surveys. Because of the observers' ability to detect large cetaceans located farther than 9 km from the aircraft, the Turbo Commander flew every-other transect line, resulting in 9.5 km spacing.

A downward-pointing Nikon D810 high-resolution digital camera with a 21-mm Zeiss Distagon lens was attached to a mount installed in the belly port of the Turbo Commander. The lens was directly exposed to the outside air. The camera automatically collected images every 2 s, during which time the aircraft traveled approximately 118 m. A parcel of water on the surface of the ocean was visible in at least three consecutive images, depending on aircraft altitude. Metadata automatically recorded for each image included latitude, longitude, and altitude. The Zeiss lens is capable of achieving a sharper focus than the Nikkor lens used on the UAV due to high-quality glass and anti-glare coating on the former. However, the differences between the lenses at the distances to our targets were negligible in terms of the ability to detect or identify animals. The Zeiss lens was too heavy and long to use in the UAV.

Aviation safety

Safety was the primary concern of project personnel. Several tools were used to enhance the safety of, and minimize risk to, non-participating and participating aircraft during field operations; these tools are comprehensively discussed in Angliss et al. (2018). The UAS and ASAMM Turbo Commander flights were synchronized in time and space to obtain independent, replicate samples of cetaceans in the study area. Surveys from manned and unmanned platforms did not directly overlap spatially and temporally to maintain safety of flight. The two platforms operated as close as safely possible (Angliss et al. 2018).

Image processing methods

Detailed image processing protocols are provided in supplementary data A.[2] Digital images from the UAS and Turbo Commander flights were visually reviewed by three photo analysts with considerable expertise as marine mammal observers during visual aerial surveys for arctic marine mammals. Only images with midpoints located within

[2]Supplementary data are available with the article through the journal Web site at http://nrcresearchpress.com/doi/suppl/10.1139/juvs-2018-0002.

1 km strips centered on transects were viewed to simplify computation of the area sampled; images collected while transiting off transect were not analyzed. The native projection for the transects was used to determine which images were located in the transect strip; that projection was defined as a Lambert azimuthal equal area projection, with center latitude 70.0°, center longitude −154.5°, false easting 0.0, and false northing 0.0. Observers did not process images that showed any portion of the horizon, or where the camera angle was obviously not perpendicular to the sea surface, as these images were taken when the aircraft was turning. Because consecutive images overlapped by approximately 33% on average, photo analysts reviewed every third image from each portion of the flight that was within the study area boundaries. Ten images out of every 30 were fully analyzed at 100% zoom, while the remaining 20 were initially analyzed at 20% zoom, with instructions to selectively zoom in on any pixels containing a cue for a potential sighting. Images from nine flights (five manned flights and four UAS flights) were reviewed in detail by only a single photo analyst. Images from one UAS flight were reviewed independently by two photo analysts for an ongoing analysis to estimate detection probability. The lead photo analyst reviewed all images identified as containing definite or possible sightings to confirm species and group size, and to make a final determination on objects that were initially judged without certainty to be marine mammals. All marine mammal sightings were confirmed by two or more experienced marine mammal observers.

The final processed imagery database included the following fields: aircraft type; image filename; latitude, longitude, and altitude; date and time (GMT); impediments to visibility, Beaufort Sea State, percent of the image covered by glare, and type of glare present; whether the image was viewed at full-screen resolution or zoomed to 100% of the image size; sighting number; species identification; an ordinal variable on sighting and species identification confidence; best, high, and low estimates of group size; number of calves present; position of the sighting in *x*- and *y*-coordinates within the frame of reference of the image; length (pixels) of the animal; percentage of the image obscured by precipitation; notes if the image was not taken during level flight; and the amount of time it took to process a batch of 10 images.

Analytical methods

All analyses were conducted using R version 3.3.2 (R Core Team 2016). Geospatial analyses were conducted using R packages sp (Pebesma and Bivand 2005; Bivand et al. 2013), maptools (Bivand and Lewin-Koh 2017), rgeos (Bivand and Rundel 2017), rgdal (Bivand et al. 2016), raster (Hijmans 2016), ncdf4 (Pierce 2015), and fields (Nychka et al. 2015).

Throughout the text, we refer to "density"; however, results are presented both in terms of density and number of individual animals to facilitate interpretation. All density computations were standardized as number of animals per square kilometre. Density estimates were converted to estimates of the number of whales of each species present in each sector by multiplying estimated density by the corresponding sector area.

Density estimates were not corrected for availability bias resulting from the animals' surfacing and diving behaviors or for the photo analysts' perception bias (Marsh and Sinclair 1989). Additional data need to be collected to compute correction factors for the marine mammal observers' perception bias near the trackline; therefore, this bias was not addressed. Analyses of cetacean behavior from satellite telemetry and aerial behavior studies, and aircraft field of view data are being used to compute availability bias correction factors specific to the ASAMM line-transect surveys. Investigations into adjusting the sightings in the imagery for perception or availability bias are also underway.

Density estimation from the UAS and Turbo Commander imagery

Density was estimated separately for each combination of: species (bowhead whale, gray whale, or beluga), aircraft type (Turbo Commander or UAS), and sector (west or east) of the study area. Separate density estimates were derived for the east and west sectors because they were known a priori to represent distinct habitats, and it was assumed that densities would not be constant throughout the entire UAS study area. Spatial modeling methods can incorporate sightings and effort off transects; however, the sample sizes in our imagery were not large enough to create spatial models that would enable use of off-transect data.

Density estimates were based on the total visible area in each image, which was calculated as the total image area multiplied by the proportion of the surface area visible. Images with <50% surface area visible (due to precipitation) were considered to contain minimal information and could potentially introduce biases into the analysis, so they were omitted from the density analyses. Because of the relatively small sample size, we were unable to examine the effects of Beaufort Sea State or glare on detection probabilities.

The total area of each image was calculated as the product of the horizontal coverage (coverage.h, in metres) and vertical coverage (coverage.v, in metres), divided by 1×10^6 to produce a value in square kilometres. Horizontal and vertical coverage were calculated as follows:

$$\text{(1)} \quad \text{coverage.h} = \left(\frac{\text{sensor.h}}{f}\right)\text{alt}$$

$$\text{(2)} \quad \text{coverage.v} = \left(\frac{\text{sensor.v}}{f}\right)\text{alt}$$

where sensor.h is the horizontal dimension (mm) of the camera's sensor, sensor.v is the vertical dimension (mm) of the camera's sensor, f is the focal length (mm) of the lens, and alt is the survey altitude (m).

Density estimates were derived for each species from the imagery as

$$\text{(3)} \quad \hat{D}_{p,\text{sp}} = \frac{\sum_{i=1}^{k}\sum_{j=1}^{m} n_{i,j,p,\text{sp}}}{\sum_{i=1}^{k}\sum_{j=1}^{m} a_{p,i,j}}$$

where $\hat{D}$ is the estimated density; p is the platform type (UAS or Turbo Commander); sp is the species; k is the total number of unique transect lines covered by each platform;[3] m is the total number of replicates of transect line i covered by each platform; $n_{i,j,p,\text{sp}}$ is the number of individuals of species sp in imagery collected by platform p on replicate j of transect i; and $a_{p,i,j}$ is the total visible area in replicate j of transect i from platform p.

Coefficients of variation (CV) for the density estimates were estimated using a modified version of the R2 estimator from Fewster et al. (2009), based on input from Fewster (R. Fewster personal communication to M. Ferguson on 7 October 2016). The R2 variances in the density estimates for each species × platform × sector were estimated as

$$\text{(4)} \quad \widehat{\text{var}_{\text{R2}}}(D) = \frac{k}{A^2(k-1)}\sum_{i=1}^{k}\left(\sum_{j=1}^{m} a_{i,j}\right)^2\left(\frac{\sum_{j=1}^{m} n_{i,j}}{\sum_{j=1}^{m} a_{i,j}} - \frac{n_{\text{tot}}}{A}\right)^2$$

[3]The variables k and m are platform-specific, but the "p" subscript is omitted from k and m throughout the manuscript for simplicity.

where $A = \sum_{i=1}^{k} \sum_{j=1}^{m} a_{p,i,j}$ is the total visible area covered by platform p and $n_{\text{tot}} = \sum_{i=1}^{k} \sum_{j=1}^{m} n_{i,j,p,\text{sp}}$ is the total number of individuals of species sp detected in imagery from platform p.

The $\widehat{\text{CV}(D)}$ for each species and platform was estimated as

$$\widehat{\text{CV}(D)} = \frac{\sqrt{\widehat{\text{var}_{\text{R2}}(D)}}}{\hat{D}_{p,\text{sp}}} \quad (5)$$

Because sector area is a constant, $\widehat{\text{CV}(D)}$ equals $\widehat{\text{CV}(N)}$, where $\hat{N}$ is the estimated number of whales.

Density estimation from ASAMM marine mammal observer data

Density and corresponding CV estimates were derived for bowhead whales and belugas using standard distance sampling methods, and for bowhead whales using both standard distance sampling and density surface modeling methods. There were no sightings of gray whales that met the data filter criteria for these analyses (supplementary data B[2]). There were too few beluga sightings, and they were too tightly clustered to construct a density surface model. The data filters used for each of the methods described herein are illustrated in supplementary data B (Fig. B1).[2]

Geospatial analyses used to estimate density from the ASAMM data were conducted in an equidistant conic projection defined as follows: first standard parallel 71.17°, second standard parallel 71.86°, latitude of origin 71.51°, longitude of origin −156.64°, false easting 0.0, and false northing 0.0.

Standard distance sampling methods for line transects extrapolate from the sightings observed on transect lines to an estimate of the number or density of animals in the study area or geographic strata by fitting a detection function to estimate the effective area surveyed and using design-based inference to extrapolate to the survey region (Buckland et al. 2001; Thomas et al. 2010). The detection function acknowledges that observers' ability to detect animals decreases with distance from the trackline and possibly other factors (Marques and Buckland 2003). Assuming that the probability of detecting animals located directly on the trackline is certain (i.e., $g(0) = 1.0$), the standard distance sampling density estimator for animals located in groups (Buckland et al. 2001) is

$$\hat{D} = \frac{n\widehat{E(s)}}{2L\hat{\mu}} = \frac{n\widehat{E(s)}}{2Lw\hat{p}_{\text{a}}} \quad (6)$$

where $\widehat{E(s)}$ is the expected group size, L is the total transect length surveyed, $\hat{\mu}$ is the estimated effective strip half-width, w is the right-truncation distance used to fit the detection function, and $\hat{p}_{\text{a}}$ is the estimated unconditional probability of detecting an animal in a strip of area $2wL$.

The effective strip half-width is the distance on one side of the trackline that would contain the same number of sightings if detection probability were equal to 1.0 as were actually detected during the survey. $\hat{\mu}$ equals the integral of the detection function over the range of the distance surveyed on each side of the trackline. For analyses that accounted for variable visibility range due to precipitation, which effectively resulted in a variable width searched along transects (quantified by VisX.km), $\hat{\mu}$ and $\hat{p}_{\text{a}}$ were computed using the modified methods described in Buckland et al. (2001, eq. (6.42)) and in supplementary data B.[2] The numeric variable VisX.km was derived for each record in the ASAMM database by first converting the categorical values for the left and right side visibility ranges into numeric values

corresponding to the maximum range for the category (e.g., "2–3 km" became 3.0 km), and then averaging the numeric values on both sides of the aircraft.

The number of sightings that met the relevant data filtering criteria (supplementary data B, Fig. B1[2]) during the five ASAMM flights conducted in the UAS survey area during this study (37 bowhead whale groups and 12 beluga groups) were insufficient to estimate reliable detection functions for bowhead whales and belugas. Buckland et al. (2001) note that it is the absolute size of the sample, not the fraction of the population sampled, that is the relevant sample size, and suggest that a practical minimum for reliable estimation of the detection function is 60–80 sightings. Nevertheless, for illustrative purposes, we present bowhead whale density estimates derived using standard distance sampling methods and density surface models that incorporated detection functions created using the limited dataset (supplementary data B[2]).

The historical ASAMM dataset was used to create more reliable detection function models for both bowhead whales and belugas (supplementary data B[2]). From 2009 through 2015, ASAMM surveys were conducted using comparable Turbo Commander aircraft, the same standardized line-transect survey protocols, and many of the same observers as ASAMM used during the UAS survey period. Detection functions built with the historical data incorporated sightings from across the entire ASAMM study area. The best bowhead whale detection function model based on the historical dataset, which was used to derive density estimates using both standard distance sampling methods and density surface modeling methods, included depth and group size covariates. The best beluga detection function model included longitude, a categorical variable related to percent cover of sea ice, and a categorical variable distinguishing between group sizes $\leq$10 versus >10. Depth and longitude variables were considered proxies for unmeasured variables related to differences in habitat or behavior across the ASAMM study area that affected detectability.

In the standard distance sampling analysis, density and CV(D) were estimated using the mrds package (Laake et al. 2016) in R. Data filters used to estimate density via standard distance sampling methods were identical to those used to construct the detection function models (supplementary data B[2]), with the exception that only transect sightings collected during ASAMM survey flights in the UAS study area, following the UAS transect lines, during the UAS field season were used (supplementary data B, Fig. B1[2]). In the analyses that accounted for the variable width searched along transects, the area sampled was calculated as the product of transect length and VisX.km (e.g., eq. (10)). Encounter rate variance calculations used the R2 estimator (Fewster et al. 2009). The sample unit used in this analysis was transect; therefore, effort and sighting data collected on a single transect over multiple days were pooled.

Density surface modeling incorporates spatially referenced data to model the variation in animal density across a spatial grid comprising high-resolution cells (e.g., squares or hexagons). The only spatially referenced data we considered were projected geographic coordinates because we were interested in explaining the observed spatial variation in density within a well-sampled study area rather than directly investigating ecological factors shaping that variability or extrapolating the predictions beyond the spatial or temporal extent of the surveys.

We implemented two-stage density surface modeling methods, wherein the detection function is parameterized independent of the spatial model used to estimate density (Miller et al. 2013). The detection functions used in the density surface models were the same models used in the standard distance sampling analysis (supplementary data B[2]). Data filters used to generate the data subset for spatial modeling were identical to those used to estimate density in the standard distance sampling analysis, with the exception that sightings and effort from both transect and search survey modes were included in

the spatial models (supplementary data B, Fig. B1[2]). Spatial models were created using generalized additive modeling methods from package mgcv (Wood 2006), parameterized by a negative binomial distribution (function "negbin" in the language of mgcv) with a natural logarithmic link function. The generalized cross-validation score was used for smoothing parameter estimation, with the gamma parameter set to 1.4 to control for overfitting (Wood 2006). Quasi-Poisson and Tweedie (Tweedie 1984; Dunn and Smith 2005) models, and negative binomial models based on the "nb" function were also considered, but examination of model residuals (Ver Hoef and Boveng 2007) and maps of predictions suggested that the negbin function provided a better fit to the data.

Miller et al. (2013) describe methods in which the analytical sample unit for constructing spatial models is a transect segment created by sequentially chopping transects into equidistant pieces, beginning with the start of a given transect and continuing to its endpoint. Effort and sightings in one transect segment compose a single sample unit. The parameterized spatial model is then applied to a georeferenced grid to extrapolate density predictions across the entire surface. We defined an analytical sample unit for constructing our spatial models to be one 5 km hexagonal cell of the spatial grid encompassing the study area; therefore, the sample units used to construct the spatial model were identical to those for which predictions are needed. In this case, survey effort and sightings were summarized into cells as if a honeycomb matching the spatial grid were dropped onto the georeferenced survey data, and all of the sightings and effort contained within each cell made up one sample.

Two types of spatial models were built, depending on whether information specific to each sample unit (i.e., hexagonal cell) or each sighting was used to parameterize the detection function (Miller et al. 2013). For analyses using the limited dataset, when only cell-level covariates were used in the detection function and it was assumed that the search width was constant, the count-response spatial model was used to estimate density

$$\ln(E(\text{ind}_c)) = \beta_0 + f(X_c, Y_c) + \text{offset}(\ln(2\hat{\mu}_c L_c)) \quad (7)$$

where ind_c is the random variable for the number of individual whales in cell c, with ind_c referring to the associated observations and $E(\text{ind}_c)$ the expected value (mean) of ind_c; β_0 is the intercept; X_c is the projected longitude of the midpoint of cell c; Y_c is the projected latitude of the midpoint of cell c; $f(\cdot)$ is the smooth function (Wood et al. 2008) of location covariates used to describe whale density (this function is parameterized in the model-fitting process); $\hat{\mu}_c$ is the estimated effective strip half-width of cell c; and L_c is the length (km) of transect effort in cell c.

The smooth function used in the best model was a thin plate regression spline with extra shrinkage. The extra shrinkage allows the spline parameters to shrink to zero, if necessary, during estimation (Wood 2006). The offset term accounts for spatially heterogeneous survey effort across the study area and is treated as a constant during the model-fitting process. Models based on tensor products and soap film smooths were evaluated but did not perform as well as the thin plate regression spline models, presumably because of data sparsity.

For analyses using the historical dataset, when covariates specific to each sighting were used in the detection function or the variable search width was incorporated into the detection function model, the abundance-response model was used

$$\ln(E(\hat{N}_c)) = \beta_0 + f(X_c, Y_c) + \text{offset}(\ln(a_c)) \quad (8)$$

where $\hat{N}_c$ is the estimated abundance in cell c

$$\hat{N}_c = \sum_r \frac{\text{ind}_{cr}}{\hat{p}_{cr}} \quad (9)$$

where r is the an index identifying unique sightings; $\hat{p}_{cr}$ is the estimated unconditional probability of detecting sighting r located within w distance of the trackline in cell c; and a_c is the area sampled in cell c, computed as

$$a_c = 2\sum_v \text{VisX.km}_v L_{cv} \quad (10)$$

where v is an index identifying unique values of VisX.km and L_{cv} is the length of survey effort covered in cell c under visibility conditions VisX.km_v.

The predicted number of bowhead whales in each sector was computed by multiplying the area of each hexagonal cell contained within each sector by the corresponding density estimate for the cell, and then summing across cells in each sector.

Estimates of CV(D) for the spatial model predictions were made using the delta method to combine uncertainty from the spatial model with that from the detection function, based on the assumption that these models are independent (Buckland et al. 2001). Estimates of spatial model uncertainty, CV(gam), were calculated using the dsm.var.gam function from the dsm package (Miller et al. 2017). Detection function uncertainty, represented by $\text{CV}(\hat{p}_a)$, was computed as the standard error of $\hat{p}_a$ divided by $\hat{p}_a$. Applying the delta method,

$$\text{CV}(D) = \sqrt{[\text{CV}(\text{gam})]^2 + [\text{CV}(\hat{p}_a)]^2} \quad (11)$$

Sightings of large cetaceans unidentified to species were used to compute a "large cetacean" species identification bias correction factor, $p(\text{ID}) = 1 - p(\text{unid})$ (J. Laake, AFSC, personal communication to M. Ferguson on 3 May 2016). The variable p(unid) is the probability of recording an unidentified large cetacean in the strip (dx) located parallel to the trackline in which detectability is similar across all large cetacean species. Based on the histograms of bowhead and gray whale sightings made by ASAMM observers from 2009 through 2015 (supplementary data B[2] and MML unpublished data), dx was defined as the strip spanning 250–550 m perpendicular to the trackline. p(unid) was computed as follows:

$$p(\text{unid}) = \frac{n_{\text{unid, dx}}}{\sum_i n_{i,\text{dx}}} \quad (12)$$

where i is the species category corresponding to bowhead whale, gray whale, or unidentified large cetacean; dx is the strip located near the trackline in which detectability is similar across all species; and n is the number of sightings by airborne marine mammal observers during the UAS survey period.

To correct for species identification bias, the estimated densities of bowhead whales derived from the standard distance analysis and both spatial models were each divided by p(ID).

Results

Weather was conducive to surveying on six (35%) out of the 18 days spanning 21 August to 7 September 2015, beginning with when the UAS was operational (Angliss et al. 2018). The weather in the study area was highly variable in space and time. Conditions included fog, haze, mist, drizzle, rain and snow squalls, low cloud ceilings, and coastal flooding resulting in the declaration of a State of Emergency, with occasional periods of acceptable

Fig. 2. Location of UAS survey effort, total sightings from the UAS imagery database (Table 1), and sightings from the UAS imagery database that were used to estimate density (Table 2). Symbols overlap for nearby sightings.

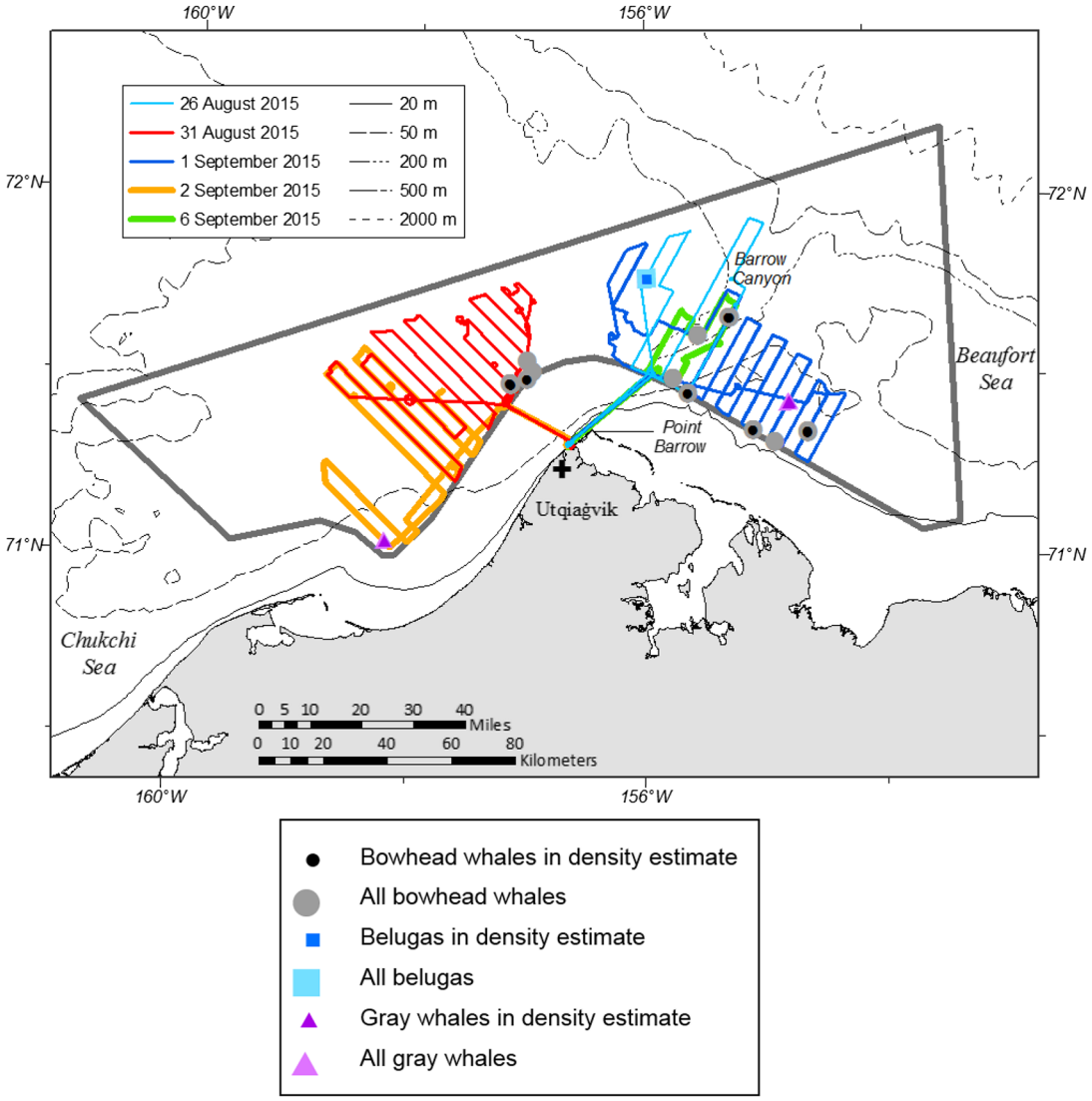

ceilings and no precipitation when flights could be conducted (Angliss et al. 2018). Although one of the project's field objectives was to cover each transect line at least once by each aircraft, weather limitations resulted in some lines being sampled multiple times and others not being sampled at all (Figs. 2, 3, and 4).

The UAS conducted five survey flights consisting of a single flight each day on five days: 26 and 31 August, and 1, 2, and 6 September. UAS flights ranged from 1.6 to 6.0 h duration, for a total of 21.8 flight hours covering 2012 km in the study area (Fig. 2) (Angliss et al. 2018). At no time were two UAVs airborne simultaneously. Of the 20 568 total images collected by the UAS in the study area (Angliss et al. 2018), 6857 (33.3%) were processed by photo analysts. During the review of every third image from each flight, photo analysts sighted 14 bowhead whale groups (totaling 15 whales), one group of six belugas, and three lone gray whales

Fig. 3. Location of Turbo Commander survey effort, total sightings from the aircraft's imagery database (Table 1), and sightings from the aircraft's imagery database that were used to estimate density (Table 2). Symbols overlap for nearby sightings.

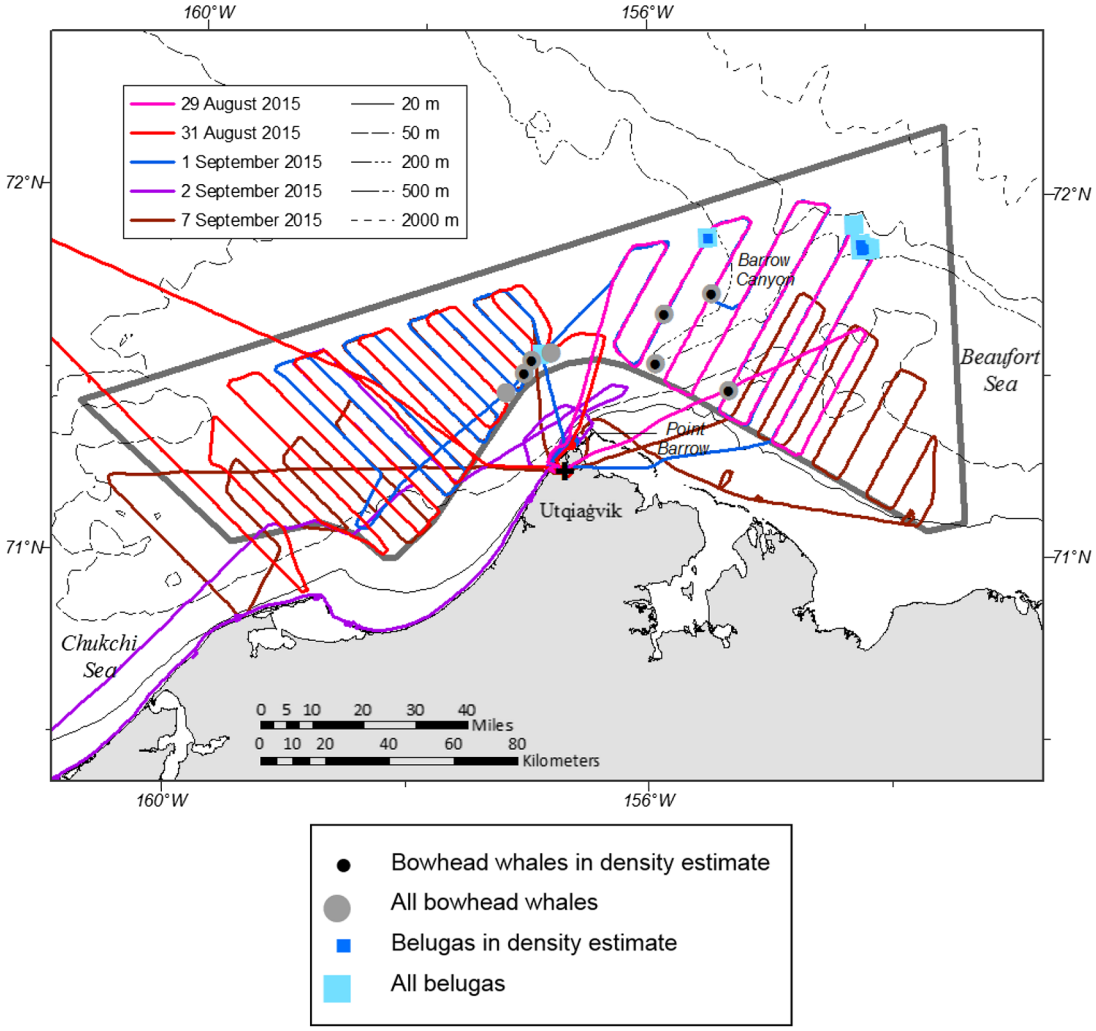

(Table 1; Fig. 2). The only calf sighted in any of the imagery from either aircraft was a bowhead whale calf associated with an adult female in an image taken from the UAS while turning, and was therefore omitted from statistical analysis.

The Turbo Commander also conducted five survey flights on the UAS transect lines during five separate days: 29 and 31 August, and 1, 2, and 7 September (Figs. 3 and 4). Survey effort in the study area ranged in duration from 1.3 to 4.8 h, totaling 17.9 h and 3582 km (Angliss et al. 2018). In total, 23 580 images were collected from the vertical camera aboard the Turbo Commander in the study area (Angliss et al. 2018), and 9776 (41.5%) were processed. The proportions of individuals of each species observed were similar across platforms, with bowhead whales generally the most frequently observed and gray whales the least. Because of the small area covered (hence, small sample sizes) in the imagery and patchy distribution of the cetaceans in the study area, the number of individuals observed and species composition were not identical across platforms and observation methods.

Fig. 4. Location of Turbo Commander survey effort, total sightings from the marine mammal observers' database (Table 1), and sightings from the observers' database that were used to estimate density by standard distance sampling methods using either the historical or limited dataset for the detection function (Table 2). Symbols overlap for nearby sightings.

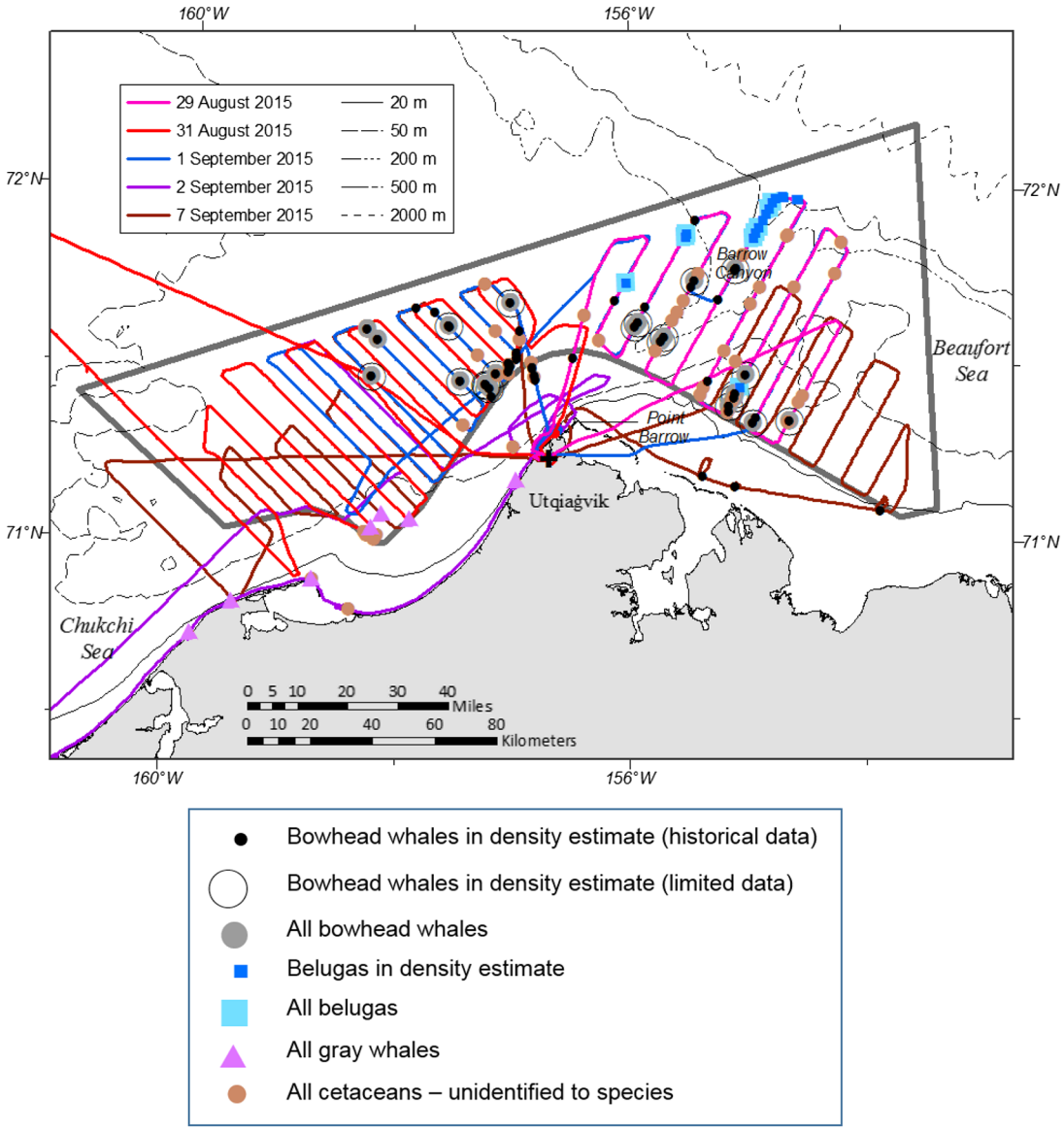

Photo analysts detected eight lone bowhead whales and 11 beluga groups totaling 16 whales (Table 1; Fig. 3). No gray whales and no calves were detected in images from the Turbo Commander. Marine mammal observers detected 53 bowhead whale groups totaling 61 whales, 18 beluga groups totaling 54 whales, 9 gray whale groups totaling 9 whales, and 42 groups totaling 48 cetaceans that could not be identified to species (Table 1; Fig. 4). This is a considerably higher proportion of cetaceans not identified to species compared to typical ASAMM flights conducted in closing mode (when the aircraft is allowed to circle sightings), but only one of those sightings was close to the aircraft, in the strip located

Table 1. Total number of whale sightings and individual whales detected in imagery from the UAS and Turbo Commander and by the marine mammal observers aboard the Turbo Commander during all survey effort (i.e., while transiting and on transect).

	UAS images		Turbo Commander images		Marine mammal observer data	
Species	No. of sightings	No. of whales	No. of sightings	No. of whales	No. of sightings	No. of whales
Beluga	1	6	11	16	18	54
Bowhead whale	14	15	8	8	53	61
Gray whale	3	3	0	0	9	9
Unidentified cetacean	0	0	0	0	42	48

250–550 m parallel to the trackline. No gray whales and 17 bowhead whales were detected in the 250–550-m strip. The resulting "large cetacean" species identification bias correction factor was 0.94; therefore, raw density estimates of bowhead whales from the marine mammal observer data were increased by a factor of 1/0.94 = 1.06, or 6%, to account for the inability to identify all large cetacean sightings to species.

Because of the different assumptions and, therefore, data filters used to construct bowhead whale detection functions from the limited versus historical dataset, sample sizes used to build the density surface models differed slightly between the count-response and the abundance-response models. The count-response spatial model was constructed from a total of 488 hexagonal cells with non-zero survey effort; 25 of those cells had bowhead whale sightings, resulting in a total of 32 bowhead whale sightings comprising 35 total whales in the model. Single whales were found in 29 of the sightings used in the count-response model, and three sightings had two whales each. The abundance-response spatial model was constructed from a total of 492 hexagonal cells with non-zero survey effort; 25 of those cells had bowhead whale sightings, and 32 bowhead whale sightings comprising 34 total whales were incorporated into the model. Single whales were found in 30 of the sightings used in the abundance-response model and two sightings had two whales each.

Bowhead whales were consistently predicted to be more numerous in the east sector than the west sector (Table 2). The patterns in predicted density were similar in the count-response (Fig. 5) and abundance-response (Fig. 6) spatial models, with the highest densities located near shore in the vicinity of Point Barrow, decreasing with increasing distance from shore. The spatial models also predicted relatively high densities over Barrow Canyon. The highest densities were shoreward of the 200 m isobath. The count-response model predicted an area of high density in the southeastern corner of the study area, due to one sighting of two whales that was filtered out of the dataset used for the abundance-response model. It is worth noting that the spatial models used information on sightings and effort from the east and west sectors to fill in the gap in survey coverage north of Utqiaġvik to generate density estimates for those cells. We believe this was reasonable because the gap in coverage was located in the middle of the survey area, comprising a relatively small area compared to the entire study area, and is known from historical studies to have cetacean habitat that is consistent with the east and west sectors, which were thoroughly surveyed. In the west sector, the estimated number of bowhead whales ranged from a low of 16 whales (based on the imagery from the Turbo Commander) to a high of 63 whales (based on standard distance sampling methods using the historical dataset). In the east sector, the estimates ranged from 38 whales (based on the imagery from the Turbo Commander) to 83 whales (based on standard distance sampling methods using the historical dataset). Variability in estimated uncertainty among analytical methods was consistent between

Table 2. Summary of density and abundance estimates for bowhead whales, belugas, and gray whales in the west and east sectors, based on imagery data from the UAS and Turbo Commander, and from marine mammal observer data collected aboard the Turbo Commander.

	West sector						East sector					
	Imagery		Marine mammal observers				Imagery		Marine mammal observers			
	UAS	Manned aircraft	Standard distance sampling (limited data)	Standard distance sampling (historical data)	Count model (limited data)	Abundance model (historical data)	UAS	Manned aircraft	Standard distance sampling (limited data)	Standard distance sampling (historical data)	Count model (limited data)	Abundance model (historical data)
Bowhead whale												
No. of whales	3	2	8	11	—	—	6	4	12	12	—	—
Area covered (km^2)	525.4	646.0	8829.8	5927.2	—	—	448.5	645.9	7166.0	5127.3	—	—
Estimated whale density	0.006	0.003	0.006	0.012	—	—	0.013	0.006	0.010	0.014	—	—
Estimated total no. of whales	29	16	32	63	35	50	82	38	63	83	60	65
CV	0.77	0.71	0.51	0.41	0.28	0.20	0.53	0.45	0.41	0.36	0.28	0.20
Beluga												
No. of whales	0	0	—	0	—	—	6	11	—	22	—	—
Area covered (km^2)	525.4	646.0	—	2207.0	—	—	448.5	645.9	—	1692.3	—	—
Estimated whale density	0.000	0.000	—	0.000	—	—	0.013	0.017	—	0.025	—	—
Estimated total no. of whales	0	0	—	0	—	—	82	105	—	152	—	—
CV	NA	NA	—	NA	—	—	1.02	0.67	—	0.72	—	—
Gray whale												
No. of whales	1	0	—	0	—	—	2	0	—	0	—	—
Area covered (km^2)	525.4	646.0	—	NA	—	—	448.5	645.9	—	NA	—	—
Estimated whale density	0.002	0.000	—	0.000	—	—	0.004	0.000	—	0.000	—	—
Estimated total no. of whales	10	0	—	0	—	—	27	0	—	0	—	—
CV	1.04	NA	—	NA	—	—	1.01	NA	—	NA	—	—

Note: Bowhead whale density estimates based on the standard distance sampling methods were adjusted for species identification bias. None of the density estimates have been adjusted for perception or availability bias. The number of whales represents the subset of whales from the sightings that met the data filter criteria for each method (supplementary data B, Fig. B1[1]). Because the marine mammal observers did not observe any gray whales within the necessary data filtering criteria, the effective area covered based on standard distance sampling methods could not be computed for gray whales. For a given species, sector, dataset, and analytical method, the coefficient of variation in estimated density (CV(D)) equals that for the estimated total number of whales (CV(N)).

Fig. 5. Bowhead whale density predictions from the count-response spatial model. The locations of the bowhead whale sightings used to build the model are also shown, according to observed group size.

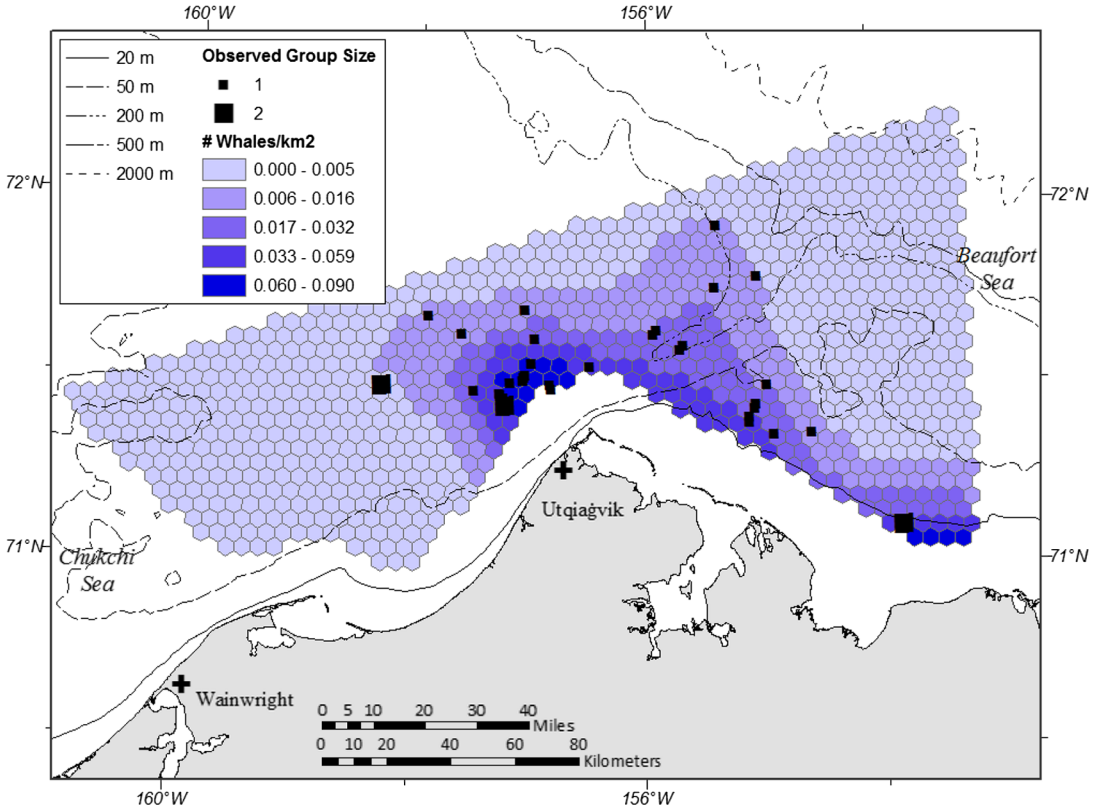

both sectors, with the spatial models having the lowest CVs (0.28 for the count-response spatial model and 0.20 for the abundance-response spatial model), standard distance sampling models having intermediate values (0.36–0.51), and estimates derived from the imagery having the highest values (0.45–0.77) (Table 2). The CVs for the spatial models can be decomposed into contributions from the spatial model and the detection function model. For the count-response model, the uncertainty due to the spatial model (CV = 0.16) was less than that from the associated detection function (CV = 0.23). For the abundance-response model, the uncertainty due to the spatial model (CV = 0.16) was greater than that from the detection function (CV = 0.11). The effective area searched, based on percentage of the water's surface visible in the imagery and sampled area for the marine mammal observers, was approximately 10 times greater for human observers than for aerial imagery (Table 2); the larger effective search area resulted in more detections and lower CVs.

Belugas were sighted in only the east sector (Table 2, Figs. 2–4). The estimated number of belugas was smallest (82 whales) for the UAS imagery and largest (152 whales) for the marine mammal observer dataset in the standard distance sampling analysis that incorporated historical data into the detection function. Estimated coefficients of variation in the density estimates were similar for the Turbo Commander imagery (0.67) and marine mammal observer dataset (0.72), and highest for the UAS dataset (1.02) (Table 2).

Gray whales were detected only in the UAS imagery (Fig. 2) and by the marine mammal observers aboard the Turbo Commander (Fig. 4); however, there were no marine mammal

Fig. 6. Bowhead whale density predictions from the abundance-response spatial model. The locations of the bowhead whale sightings used to build the model are also shown, according to group size, adjusted for the estimated unconditional detection probability, $\hat{p}_a$.

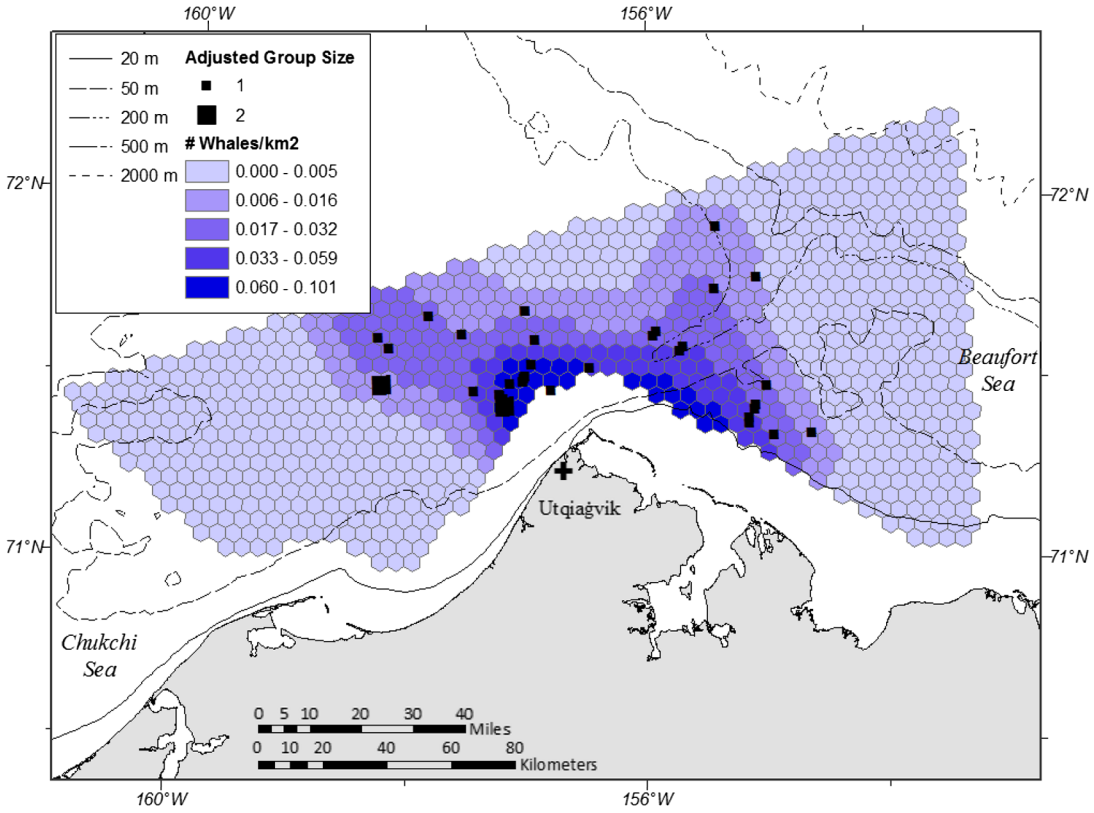

observer sightings that fit the analytical criteria for density estimation (supplementary data B and Fig. B1[2]). Therefore, estimates of the number of gray whales present were computed only from the UAS imagery, resulting in an estimate of 10 whales in the west sector and 27 whales in the east sector (Table 2). The estimated coefficients of variation in the estimated number of whales were high in the west and east sectors (1.04 and 1.01, respectively) (Table 2), reflecting the very small sample size.

Discussion

The results presented herein represent the first report of a field experiment involving simultaneous manned and unmanned aerial survey operations targeting cetaceans that provide a direct comparison among line-transect data collected by marine mammal observers onboard an aircraft, and digital photographic strip-transect data from the manned aircraft and UAV. The surveys were conducted during late summer in the Alaska Arctic, when migratory cetaceans are typically found in high abundance and weather conditions are dynamic, ranging from gale force winds, flooding rain, snow, fog, or clear skies with no measurable wind, potentially all in the course of 24 h. We analyzed each dataset separately to independently compare each method; however, a unified model that included all three sources of data could be explored as a way to utilize the strengths of each dataset to derive density estimates if a single best estimate were preferred for each species. Our

Fig. 7. Sample image of a bowhead whale from the UAS imagery taken from 272 m altitude. This whale was observed in the east sector (71.37°, –154.59°).

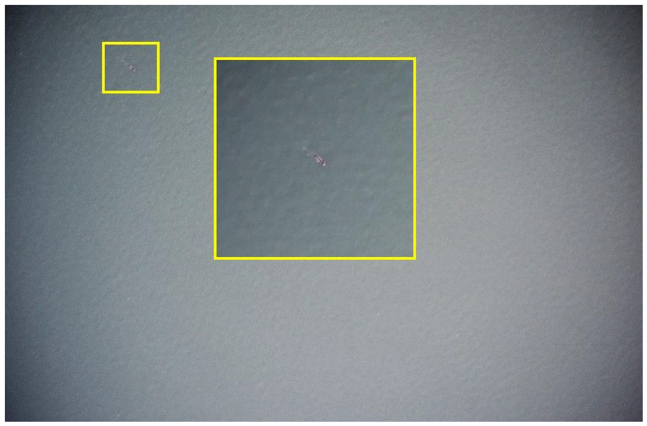

overall assessment of the methods was based on 10 performance metrics: (*i*) number of sightings made by each method; (*ii*) ability to identify sightings to species; (*iii*) ability to estimate group size; (*iv*) ability to detect calves; (*v*) precision and bias of the resulting density estimates; (*vi*) length of trackline and area sampled; (*vii*) duration of survey effort; (*viii*) analytical effort required to achieve target precision in the density estimates or to compute other derived parameters; (*ix*) monetary cost; and (*x*) non-renewable energy consumed. Each metric is discussed in this section.

The ability to study cetacean ecology unites the first five of the 10 performance metrics. In general, bowhead whales were found in higher densities and gray whales were found in lower densities than expected, and beluga densities were approximately consistent with previous years, based primarily on cumulative knowledge from the ASAMM historical database, which covers 37 field seasons (e.g., Clarke et al. 2017*a*). Due to a broader search width, the marine mammal observers sighted approximately seven times more cetaceans than were detected in either imagery dataset during a similar number of flight hours.

All methods allowed trained observers to identify bowhead whales, gray whales, belugas, and walruses. Based on the large proportion of sightings that the marine mammal observers aboard the Turbo Commander could not identify to species relative to the analogous proportion during ASAMM surveys that are conducted in closing mode (e.g., Clarke et al. 2017*a*), it is evident that implementation of passing mode line-transect surveys affected observers' ability to positively identify sightings to species. The resolutions of both imagery datasets were lower than expected due to a combination of wind, precipitation, low light, camera vibration, and the need to operate the UAV at high RPMs to mitigate icing (Angliss et al. 2018) (Fig. 7). Humpback, minke, and fin whales appear to be increasingly common in the eastern Chukchi Sea (Clarke et al. 2013; Brower et al. 2017*a*); improved image resolution may be needed to differentiate these species and certainly would be required to differentiate smaller cetaceans, such as harbor porpoise, Dall's porpoise, or pinniped species. Higher resolution could be achieved by modifying the camera mounting system to dampen vibrations. A lens with a longer focal length would also produce a higher resolution image, although at the expense of a narrower strip width and, hence, a smaller sampled area.

Small sample sizes limited our ability to determine whether the methods affected the photo analysts' or ASAMM marine mammal observers' ability to estimate group size or detect calves. In the imagery, whale group sizes ranged from one to six whales (belugas

were found in the largest groups), and only one calf, a bowhead whale, was detected. Group size estimates for cetacean sightings made by the ASAMM observers during the study period ranged from one to seven animals, with the largest groups being belugas. The ASAMM observers sighted eight beluga calves and one bowhead whale calf during the study period. Based on information in the ASAMM historical database, we know that observers detect only approximately 25% of bowhead whale calves present upon initially sighting bowhead whales (e.g., Clarke et al. 2017*a*); in other words, in 75% of the bowhead whale sightings that included at least one calf, the calf was detected only after the aircraft circled the sighting. Therefore, conducting the line-transect surveys in passing mode during this experiment likely resulted in biased estimates of calf numbers for the marine mammal observers, and possibly also in the imagery.

For bowhead whales, the species with the most sightings across all methods, there was a consistent pattern in the magnitude of the estimates of uncertainty for the density estimates in the west and east sectors, with the spatial modeling methods having the lowest CVs, followed by standard distance sampling with intermediate values, and photographic strip-transect methods having the highest CVs. In this study area, lowering the CVs of the density estimates derived from the UAS imagery to be comparable to the analogous CVs from the marine mammal observer dataset would have required approximately double the number of flight hours on the UAS. This study had planned to meet that target number of flight hours by conducting flights with two UAS simultaneously, but dual operations were not possible due to weather and logistical limitations. We adapted Fewster et al.'s (2009) R2 estimator for encounter rate variance to compute the CVs in the density estimates derived from the imagery. This was necessary because the area captured in the digital images was not consistent throughout each transect because the UAS had to vary its altitude to avoid clouds. Estimation of availability and perception biases in the density estimates from all three methods is in progress, but requires collection of additional data.

The next three performance metrics address the relative efficiency of each method: (*vi*) length of trackline and area sampled; (*vii*) duration of survey effort; and (*viii*) analytical effort required to achieve target precision in the density estimates or to compute other derived parameters. The Turbo Commander covered more distance (3582 km versus 2012 km) and ASAMM observers effectively surveyed over 10 times as much area (e.g., >11 000 km^2 sampled for bowhead whales by marine mammal observers versus ~1000 km^2 analyzed in UAV imagery) in the study area compared to the UAS in approximately the same number of flight hours.

Although photographic data provide an excellent permanent record of the strip-transect survey and allow observers unlimited time to review each snapshot, analyzing the photos to determine whether animals are present, identify sightings to species, and determine group size is labor- and time-intensive if done manually (Hodgson et al. 2013; Koski et al. 2013; Taylor et al. 2014). Simultaneous collection of infrared and high-resolution electro-optical digital imagery has successfully accelerated the processing time of the latter for detecting ice seals hauled out on ice (Sigler et al. 2015) because reliable auto-detection algorithms based on the infrared signals have been developed. However, infrared sensors are not yet able to reliably detect bowhead whales due to their thick blubber, which insulates their core from the arctic environment. In our study, photo analysts spent a total of 332.5 h to manually process and search every third image from the Turbo Commander and UAS imagery for large cetaceans, averaging 6.9 h of photo processing time per flight hour. Not included in that estimate is the considerable amount of time required to download and backup the imagery. In comparison, the preliminary round of in-field editing of the ASAMM line-transect data, which involves thorough review of the database by two

Table 3. Commensurate costs required to collect, process, archive, and analyze data during the 2015 UAS and Turbo Commander strip-transect, and Turbo Commander line-transect aerial surveys.

	UAS photo strip-transect	Turbo Commander photo strip-transect	Turbo Commander line-transect
Field work and planning	$$$$	$$	$
In-kind contributions	$$$	—	$
Post-field work expenses	$	$	$$
Total	$$$$$	$$	$$$

Note: $, <$150 000 US dollars (USD); $$, $150 000–250 000 USD; $$$, $250 000–1 000 000 USD; $$$$, $1 000 000–2 000 000 USD; $$$$$, >$2 000 000 USD.

ASAMM personnel, is completed within 2 h of the aircraft landing after each survey flight. At that stage, the data may be used in preliminary analyses. The final post-season quality assurance/quality control of the ASAMM database takes approximately 100 h to edit 100 flights, averaging 11.2 min quality assurance/quality control per flight hour.

A common belief is that UAS will be less expensive than manned aircraft to meet the same goal. Therefore, the final performance metrics we evaluated were the commensurate costs required to collect, process, archive, and analyze data to derive estimates of cetacean density and associated uncertainty. These costs could be based on time, as presented above, money (Table 3), or non-renewable energy. To compute the monetary cost of the line-transect marine mammal observer surveys, we included the following items: labor, travel, and per diem for the science crew, including pre-season preparation, field work, and post-season wrap-up; aircraft usage fees (e.g., pilot labor, travel, and per diem; aircraft maintenance and repair) and fuel; and scientific communications and equipment (e.g., survey laptop, satellite telephone service). The cost estimate for the photo strip-transect survey aboard the Turbo Commander included the following: aircraft usage fees (e.g., pilot labor, travel, and per diem; aircraft maintenance and repair) and fuel; camera mount; scientific equipment (e.g., cameras, lenses, data storage, computers, monitors, software, resolution targets); and labor for post-season image analysis and archiving. The cost estimate for the UAS survey included the following: outreach; bear guards and bear spray; landing craft to offload personnel and equipment from the ship; logistics for Utqiaġvik field work; scientific equipment and communications (e.g., cameras, lenses, data storage, computers, monitors, software, resolution targets, satellite and cellular telephone services); materials for UAS shipboard and land operations and payload integration; UAS usage fees; in-kind contributions provided by the Navy and NOAA to transport UAS equipment between Dahlgren and Utqiaġvik and use the RV *Fairweather*, respectively; and labor for post-season image analysis and archiving. Overall, the monetary cost of the 2015 marine mammal observer surveys was 9.4% the cost of the UAS component, and was approximately 68.5% the cost of the photo strip-transect survey aboard the Turbo Commander. We expect that the costs of long-range UAS surveys will come down over time as equipment becomes less expensive and less logistically complicated, and as some of the workflow becomes automated. For this project, in terms of information collected per dollar spent, using marine mammal observers to collect line-transect survey data while airborne was considerably less expensive, generated many more sightings, and resulted in more precise density estimates than either image-based method in this study.

A brief consideration of fuel consumption required to conduct each type of survey suggests that the comparison is not straightforward. The Turbo Commander burns approximately 80 gallons of fuel per hour, whereas the UAS burns approximately 0.05 gallons of fuel per hour. Nevertheless, activities necessary to support our UAS operations consumed

additional fuel. The research vessel *Fairweather* required a considerable amount of fuel to transit to the study area from Nome, Alaska; provide operational support for the UAS project; and return to port in Kodiak, Alaska. Furthermore, the C130 used to transport the UAS to Utqiaġvik burned fuel at a high rate. When indirect fuel consumption is considered, the manned aircraft operations required less fuel than the UAS operations.

One noteworthy difference between manned and unmanned aircraft is that the former are explicitly and painstakingly designed to safely return to land at the end of every flight, whereas the latter were designed to be expendable. This difference has implications in survey planning because it is important to have spare UAVs in the event that one has an unintentional water landing and cannot be recovered. Damage or loss to a UAV would have required a stand-down to review procedures, which could have resulted in lost survey days. In addition, the need for spare UAVs increases the overall project costs.

Multiple examples exist where UAS have been highly successful and have enabled researchers to collect novel data or data in locations or times that were previously inaccessible (e.g., Curry et al. 2004; Acevedo-Whitehouse et al. 2010; Fritz 2012; Knuth et al. 2013; Durban et al. 2015; Sweeney et al. 2016). However, based on the evidence encapsulated in the performance metrics summarized above, we conclude that it is premature to replace manned aerial surveys with UAS if the goal of the survey is to collect broad-scale arctic cetacean abundance or density estimates. This conclusion is based primarily on five factors: First, the technology available and used to enable manned and unmanned aircraft to fly simultaneously in close proximity in non-segregated airspace are insufficient due to the limitations of TCAS and the difficulties of visually detecting a small UAS flying at high closure rates (Angliss et al. 2018). Second, the sample sizes we obtained with the UAS were too small to reach acceptable levels of uncertainty in the density estimates. Furthermore, the raw number of sightings could be a critical factor if the goal of the survey is to mitigate, via real-time detection of animals, potential risks to marine mammals due to an anthropogenic activity, such as a military exercise or commercial seismic survey. Low sample sizes could be alleviated by flying longer (pending adequate weather), or collecting data from multiple sensors on a single UAV or on multiple UAVs flying simultaneously. Nevertheless, additional data mean additional processing time, and additional UAVs result in increased air traffic and enhanced probability of mid-air collisions. Third, the financial cost of a long-range UAS survey would be prohibitive to most wildlife managers' or ecologists' budgets. Fourth, manually processing imagery takes considerable time and money, and this is a significant hurdle to overcome without reliable auto-detection algorithms for large cetaceans (although this is a subject of current research and the cost is very likely to decrease). Finally, additional weatherproofing would be required to make UAS reliable platforms in extreme environments like the Arctic (Angliss et al. 2018).

As operational and analytical efficiency of UAS-based surveys increase, financial burdens will decrease. Development and mass production of UAS that are more weather resistant and easy to transport, and development of reliable auto-detection software for cetaceans, would reduce the costs of UAS-based surveys considerably. Ultimately, the question of whether UAS can replace or augment manned aircraft for conducting aerial surveys does not have a single answer. Rather, a lengthy list of questions should be addressed to determine whether a given UAS platform will likely meet a project's safety, scientific, and logistical needs.

Conclusions

Marine mammal observers' ability to detect motion, perceive patterns and colors, recognize target images in a visually complex field of view, and focus near and far are unmatched

by currently available optical sensors and software packages. Pilots and marine mammal observers in conventional aircraft provide real-time situational awareness of the survey process, allowing first-hand assessment of environmental conditions, their location relative to other traffic in the airspace, and the surrounding ecosystem. This situational awareness increases the probability of success by minimizing time spent in poor weather conditions that impede data collection and can affect aircraft performance. Furthermore, over a century of technology and knowledge are available to facilitate coordinating airspace among manned aircraft operating simultaneously, relying in large part on the pilot's ability to detect and avoid other aircraft. The survey crew onboard an aircraft are able to quickly integrate information from their surroundings and assess novel situations, which can lead to expedited decision-making that may affect flight safety or the value of the data being collected. Humans are impressive multi-purpose sensors. Their abilities to learn, process information, adapt to new situations, and quickly make decisions enable the survey teams to collect multiple types of data using a wide variety of tools, thereby making manned aerial surveys efficient with respect to cost and time.

At this time, the use of UAS for long-range cetacean surveys is promising, but also experimental and expensive. Further investment of time and money is required to advance technology and implement necessary safety precautions, and these improvements may shift the balance in favor of UAS for certain types of scientific aerial missions in the future.

Acknowledgements

This project was made possible by funding from the Bureau of Ocean Energy Management (BOEM), Outer Continental Shelf Region (IA No. M15PG00014), Office of Naval Research Marine Mammals and Biology Program, NOAA Unmanned Aircraft Systems Program, and NOAA Fisheries Office of Science and Technology. The ASAMM manned aerial surveys were funded by BOEM (IA No. M11PG00033). The US Navy provided additional in-kind support by flying the UAS equipment from Dahlgren, Virginia, to Utqiaġvik, Alaska, aboard a C130. NOAA provided 21 sea days on the NOAA *Fairweather* in kind. NOAA's Office of Marine and Aviation Operations and the North Slope Borough Department of Wildlife Management assisted with permitting, logistics, and planning prior to and during the field season. Invaluable information on weather for the immediate vicinity of the ground control station was provided by a portable weather station that the Office of Naval Research lent to the project and by PEMDAS NOWcast software. Shell Oil and LGL provided in-kind support to collect and process the imagery from the manned aircraft. We appreciate the hard work of the ASAMM observers and Clearwater Air and Navy UAS pilots prior to, during, and after the field season. Real-time monitoring via satellite tracking of ASAMM survey flights was provided by the US Department of the Interior. The ASAMM project is also grateful for the analytical and programming expertise provided by XeraGIS. Paul Conn, Erin Moreland, and two anonymous reviewers provided valuable feedback on a draft of this manuscript. This research was authorized under Marine Mammal Protection Act permit 14245-03, as amended and issued to the National Marine Mammal Laboratory by the NOAA Fisheries Office of Protected Resources. This research was also authorized under Marine Mammal Protection Act permit 212570-1, as amended by the US Fish and Wildlife Service. Permission to conduct the ScanEagle® mission was granted by the FAA (COA 2015-WSA-113) and Navy (COE-1100-001-12-10). Reference to trade names does not indicate endorsement by the National Marine Fisheries Service, NOAA. The findings and conclusions in this paper are those of the author(s) and do not necessarily represent the views of the National Marine Fisheries Service.

References

Acevedo-Whitehouse, K., Rocha-Gosselin, A., and Gendron, D. 2010. A novel non-invasive tool for disease surveillance of free-ranging whales and its relevance to conservation programs. Anim. Conserv. **13**: 217–225. doi: 10.1111/j.1469-1795.2009.00326.x.

Anderson, K., and Gaston, K.J. 2013. Lightweight unmanned aerial vehicles will revolutionize spatial ecology. Front. Ecol. Environ. **11**(3): 138–146. doi: 10.1890/120150.

Angliss, R.P., Ferguson, M.C., Hall, P., Helker, V., Kennedy, A., and Sformo, T. 2018. Comparing manned to unmanned aerial surveys for cetacean monitoring in the Arctic: Methods and operational results. J. Unmanned Veh. Syst. This issue. doi: 10.1139/juvs-2018-0001.

Barasona, J.A., Mulero-Pázmány, M., Acevedo, P., Negro, J.J., Torres, M.J., Gortázar, C., and Vicente, J. 2014. Unmanned aircraft systems for studying spatial abundance of ungulates: Relevance to spatial epidemiology. PLoS ONE, **9**(12): e115608. doi: 10.1371/journal.pone.0115608. PMID: 25551673.

Bivand, R.S., and Lewin-Koh, N. 2017. maptools: Tools for reading and handling spatial objects. R package version 0.9-1. Available from https://CRAN.R-project.org/package=maptools.

Bivand, R.S., and Rundel, C. 2017. rgeos: Interface to geometry engine — Open source (GEOS). R package version 0.3-22. Available from https://CRAN.R-project.org/package=rgeos.

Bivand, R.S., Pebesma, E., and Gomez-Rubio, V. 2013. Applied spatial data analysis with R. 2nd ed. Springer, New York, N.Y., USA. Available from http://www.asdar-book.org/.

Bivand, R.S., Keitt, T., and Rowlingson, B. 2016. rgdal: Bindings for the 'Geospatial' Data Abstraction Library. R package version 1.2-5. Available from https://CRAN.R-project.org/package=rgdal.

Brower, A.A., Clarke, J., and Ferguson, M. 2017*a*. Subarctic cetaceans in the eastern Chukchi Sea, 2008–2016: Population recovery, response to climate change, or increased effort? Presented to the IWC Scientific Committee, Bled, Slovenia, April 2017. Paper SC-A17-NP-04.

Brower, A.A., Ferguson, M., Schonberg, S., Jewett, S., and Clarke, J. 2017*b*. Gray whale distribution relative to benthic invertebrate biomass and abundance: Northeastern Chukchi Sea 2009–2012. Deep Sea Res., Part II, **144**: 156–174. doi: 10.1016/j.dsr2.2016.12.007.

Buckland, S.T., Anderson, D.R., Burnham, K.P., Laake, J.L., Borchers, D.L., and Thomas, L. 2001. Introduction to distance sampling: Estimating abundance of biological populations. Oxford University Press, Oxford, UK. 432 pp.

Chabot, D., Craik, S.R., and Bird, D.M. 2015. Population census of a large common tern colony with a small unmanned aircraft. PLoS ONE, **10**(4): e0122588. doi: 10.1371/journal.pone.0122588. PMID: 25874997.

Citta, J.J., Quakenbush, L.T., Okkonen, S.R., Druckenmiller, M.L., Maslowski, W., Clement-Kinney, J., George, J.C., Brower, H., Small, R.J., Ashjian, C., Harwood, L.A., and Heide-Jørgensen, M.P. 2015. Ecological characteristics of core-use areas used by Bering–Chukchi–Beaufort (BCB) bowhead whales, 2006–2012. Prog. Oceanogr. **136**: 201–222. doi: 10.1016/j.pocean.2014.08.012.

Clarke, J.T., Stafford, K., Moore, S.E., Rone, B., Aerts, L., and Crance, J. 2013. Subarctic cetaceans in the southern Chukchi Sea: Evidence of recovery or response to a changing ecosystem. Oceanography, **26**(4): 136–149. doi: 10.5670/oceanog.2013.81.

Clarke, J.T., Ferguson, M.C., Curtice, C., and Harrison, J. 2015. Biologically important areas for cetaceans within U.S. waters — Arctic region. Aquat. Mamm. **41**(1): 94–103. doi: 10.1578/AM.41.1.2015.94.

Clarke, J.T., Kennedy, A.S., and Ferguson, M.C. 2016. Bowhead and gray whale distributions, sighting rates, and habitat associations in the eastern Chukchi Sea, summer and fall 2009–15, with a retrospective comparison to 1982–91. Arctic, **69**(4): 359–377. doi: 10.14430/arctic4597.

Clarke, J.T., Brower, A.A., Ferguson, M.C., and Willoughby, A.L. 2017*a*. Distribution and relative abundance of marine mammals in the eastern Chukchi and western Beaufort Seas, 2015. Annual Report, OCS Study BOEM 2017-019. National Marine Mammal Laboratory, Alaska Fisheries Science Center, NMFS, NOAA, Seattle, Wash., USA.

Clarke, J.T., Brower, A.A., Ferguson, M.C., and Willoughby, A.L. 2017*b*. Distribution and relative abundance of marine mammals in the eastern Chukchi and western Beaufort Seas, 2016. Annual Report, OCS Study BOEM 2017-078. National Marine Mammal Laboratory, Alaska Fisheries Science Center, NMFS, NOAA, Seattle, Wash., USA.

Clarke, J.T., Ferguson, M.C., Willoughby, A.L., and Brower, A.A. 2018. Bowhead and beluga whale distributions, sighting rates, and habitat associations in the western Beaufort Sea in summer and fall 2009–16, with comparison to 1982–91. Arctic, **71**(2):4713. doi: 10.14430/arctic4713.

Curry, J., Maslanik, J., Holland, G., and Pinto, J. 2004. Applications of aerosondes in the arctic. Bull. Am. Meteorol. Soc. **85**: 1855–1862. doi: 10.1175/BAMS-85-12-1855.

Dunn, P.K., and Smith, G.K. 2005. Series evaluation of Tweedie exponential dispersion model densities. Stat. Comput. **15**: 267–280. doi: 10.1007/s11222-005-4070-y.

Durban, J.W., Fearnbach, H., Barrett-Lennard, L.G., Perryman, W.L., and Leroi, D.J. 2015. Photogrammetry of killer whales using a small hexacopter launched at sea. J. Unmanned Veh. Syst. **3**(3): 131–135. doi: 10.1139/juvs-2015-0020.

Fewster, R.M., Buckland, S.T., Burnham, K.P., Borchers, D.L., Jupp, P.E., Laake, J.L., and Thomas, L. 2009. Estimating the encounter rate variance in distance sampling. Biometrics, **65**: 225–236. doi: 10.1111/j.1541-0420.2008.01018.x. PMID: 18363772.

Fritz, L. 2012. By land, sea, and air: A collaborative Steller sea lion research cruise in the Aleutian Islands. Alaska Fisheries Science Center Quarterly Report, January–February–March. Available from http://www.afsc.noaa.gov/Quarterly/jfm2012/divrptsNMML1.htm.

Garner, G.W., Amstrup, S.C., Laake, J.L., Manly, B.F.J., McDonald, L.L., and Robertson, D.G. 1999. Marine mammal survey and assessment methods. A.A. Balkema, Rotterdam, the Netherlands and Brookfield, Vt., USA. 177 pp.
Goebel, M.E., Perryman, W.L., Hinke, J.T., Krause, D.J., Hann, N.A., Gardner, S., and LeRoi, D.J. 2015. A small unmanned aerial system for estimating abundance and size of Antarctic predators. Polar Biol. **38**(5): 619–630. doi: 10.1007/s00300-014-1625-4.
Hijmans, R.J. 2016. raster: Geographic data analysis and modeling. R package version 2.5-8. Available from https://CRAN.R-project.org/package=raster.
Hodgson, A., Kelly, N., and Peel, D. 2013. Unmanned aerial vehicles (UAVs) for surveying marine fauna: A Dugong case study. PLoS ONE, **8**(11): e79556. doi: 10.1371/journal.pone.0079556. PMID: 24223967.
Knuth, S.L., Cassano, J.J., Maslanik, J.A., Herrmann, P.D., Kernebone, P.A., Crocker, R.I., and Logan, N.J. 2013. Unmanned aircraft system measurements of the atmospheric boundary layer over Terra Nova Bay, Antarctica. Earth Syst. Sci. Data, **5**: 57–69. doi: 10.5194/essd-5-57-2013.
Koski, W.R., Zeh, J., Mocklin, J., Davis, A.R., Rugh, D.J., George, J.C., and Suydam, R. 2010. Abundance of Bering-Chukchi-Beaufort bowhead whales (*Balaena mysticetus*) in 2004 estimated from photo-identification data. J. Cetacean Res. Manage. **11**(2): 89–99.
Koski, W.R., Thomas, T.A., Funk, D.W., and Macrander, A.M. 2013. Marine mammal sightings by analysts of digital imagery versus aerial surveyors: A preliminary comparison. J. Unmanned Veh. Syst. **1**: 25–40. doi: 10.1139/juvs-2013-0015.
Koski, W.R., Gamage, G., Davis, A.R., Mathews, T., LeBlanc, B., and Ferguson, S.H. 2015. Evaluation of UAS for photographic re-identification of bowhead whales, *Balaena mysticetus*. J. Unmanned Veh. Syst. **3**: 22–29. doi: 10.1139/juvs-2014-0014.
Laake, J., Borchers, D., Thomas, L., Miller, D., and Bishop, J. 2016. mrds: Mark-recapture distance sampling. R package version 2.1.17. Available from https://CRAN.R-project.org/package=mrds.
Maire, F., Mejias, L., Hodgson, A., and Duclos, G. 2013. Detection of dugongs from unmanned aerial vehicles. *In* Proceedings of the IEEE/RSJ International Conference on Intelligent Robots and Systems 2013. Tokyo Big Sight, Tokyo, Japan. p. 2750–2756. doi: 10.1109/IROS.2013.6696745.
Marques, F.F.C., and Buckland, S.T. 2003. Incorporating covariates into standard line transect analyses. Biometrics, **59**: 924–935. doi: 10.1111/j.0006-341X.2003.00107.x. PMID: 14969471.
Marsh, H., and Sinclair, D.F. 1989. Correcting for visibility bias in strip transect aerial surveys of aquatic fauna. J. Wildl. Manage. **53**(4): 1017–1024. doi: 10.2307/3809604.
Miller, D.L., Burt, M.L., Rexstad, E.A., and Thomas, L. 2013. Spatial models for distance sampling data: Recent developments and future directions. Methods Ecol. Evol. **4**: 1001–1010. doi: 10.1111/2041-210X.12105.
Miller, D.L., Rexstad, E., Burt, L., Bravington, M.V., and Hedley, S. 2017. dsm: Density surface modelling of distance sampling data. R package version 2.2.15. Available from http://github.com/DistanceDevelopment/dsm.
Mocklin, J.A., George, J.C., Ferguson, M., Vate Brattström, L., Beaver, V., Rone, B., Christman, C., Brower, A., Shea, B., and Accardo, C. 2012*a*. Aerial photography of bowhead whales near Barrow, Alaska, during the 2011 spring migration. Presented to the International Whaling Commission Scientific Committee, Panama City, Panama. Paper SC/64/BRG3.
Mocklin, J.A., Rugh, D.J., Moore, S.E., and Angliss, R.P. 2012*b*. Using aerial photography to investigate evidence of feeding by bowhead whales. Mar. Mammal Sci. **28**(3): 602–619. doi: 10.1111/j.1748-7692.2011.00518.x.
Moreland, E.E., Cameron, M.F., Angliss, R.P., and Boveng, P.L. 2015. Evaluation of a ship-based unoccupied aircraft system (UAS) for surveys of spotted and ribbon seals in the Bering Sea pack ice. J. Unmanned Veh. Syst. **3**(3): 114–122. doi: 10.1139/juvs-2015-0012.
Mulero-Pázmány, M., Barasona, J.Á., Acevedo, P., Vicente, J., and Negro, J.J. 2015. Unmanned aircraft systems complement biologging in spatial ecology studies. Ecol. Evol. **5**(21): 4808–4818. doi: 10.1002/ece3.1744. PMID: 26640661.
Muto, M.M., Helker, V.T., Angliss, R.P., Allen, B.A., Boveng, P.L., Breiwick, J.M., Cameron, M.F., Clapham, P.J., Dahle, S.P., Dahlheim, M.E., Fadely, B.S., Ferguson, M.C., Fritz, L.W., Hobbs, R.C., Ivashchenko, Y.V., Kennedy, A.S., London, J.M., Mizroch, S.A., Ream, R.R., Richmond, E.L., Shelden, K.E.W., Towell, R.G., Wade, P.R., Waite, J.M., and Zerbini, A.N. 2017. Alaska marine mammal stock assessments, 2016. U.S. Department of Commerce, NOAA Technical Memorandum NMFS-AFSC-355. 366 pp. doi: 10.7289/V5/TM-AFSC-355.
Nychka, D., Furrer, R., Paige, J., and Sain, S. 2015. fields: Tools for spatial data. Version 8.10. Available from www.image.ucar.edu/fields.
Pebesma, E.J., and Bivand, R.S. 2005. Classes and methods for spatial data in R. R News, **5**(2). Available from https://cran.r-project.org/doc/Rnews/.
Pierce, D. 2015. ncdf4: Interface to Unidata netCDF (version 4 or earlier) format data files. R package version 1.15. Available from https://CRAN.R-project.org/package=ncdf4.
R Core Team. 2016. R: A language and environment for statistical computing. R Foundation for Statistical Computing, Vienna, Austria. Available from https://www.R-project.org/.
Richardson, W.J., and Thomson, D.H. 2002. Bowhead whale feeding in the eastern Alaskan Beaufort Sea: Update of scientific and traditional information. OCS Study MMS 2002-012; LGL Report TA2196-7. Report from LGL Ltd., King City, Ont., Canada, for US Minerals Management Service, Anchorage, Alaska and Herndon, Va., USA. Vol. 1, xliv + 420 pp.; Vol. 2, 277 pp.
Richardson, W.J., Fraker, M.A., Würsig, B., and Wells, R.S. 1985. Behaviour of bowhead whales *Balaena mysticetus* summering in the Beaufort Sea: Reactions to industrial activities. Biol. Conserv. **32**: 195–230. doi: 10.1016/0006-3207(85)90111-9.
Richardson, W.J., Würsig, B., and Greene, C.R., Jr. 1986. Reactions of bowhead whales, *Balaena mysticetus*, to seismic exploration in the Canadian Beaufort Sea. J. Acoust. Soc. Am. **79**(4): 1117–1128. doi: 10.1121/1.393384. PMID: 3700867.

Richardson, W.J., Davis, R.A., Evans, C.R., Ljungblad, D.K., and Norton, P. 1987. Summer distribution of bowhead whales, *Balaena mysticetus*, relative to oil industry activities in the Canadian Beaufort Sea, 1980–84. Arctic, **40**(2): 93–104. doi: 10.14430/arctic1753.

Rümmler, M.C., Mustafa, O., Maercker, J., Peter, H., and Esefeld, J. 2016. Measuring the influence of unmanned aerial vehicles on Adélie penguins. Polar Biol. **39**: 1329–1334. doi: 10.1007/s00300-015-1838-1.

Sarda-Palomera, F., Bota, G., Vinolo, C., Pallares, O., Sazatornil, V., Brotons, L., Gomariz, S., and Sarda, F. 2012. Fine-scale bird monitoring from light unmanned aircraft systems. Ibis, **154**: 177–183. doi: 10.1111/j.1474-919X.2011.01177.x.

Schick, R.S., and Urban, D.L. 2000. Spatial components of bowhead whale (*Balaena mysticetus*) distribution in the Alaskan Beaufort Sea. Can. J. Fish. Aquat. Sci. **57**: 2193–2200. doi: 10.1139/f00-196.

Schweder, T. 2003. Abundance estimation from multiple photo surveys: Confidence distributions and reduced likelihoods for bowhead whales off Alaska. Biometrics, **59**: 974–983. doi: 10.1111/j.0006-341X.2003.00112.x. PMID: 14969476.

Schweder, T., Sadykova, D., Rugh, D.J., and Koski, W.R. 2010. Population estimates from aerial photographic surveys of naturally and variably marked bowhead whales. J. Agric. Biol. Environ. Stat. **15**(1): 1–19. doi: 10.1007/s13253-009-0002-1.

Sigler, M., DeMaster, D., Boveng, P., Cameron, M., Moreland, E., Williams, K., and Towler, R. 2015. Advances in methods for marine mammal and fish stock assessments: Thermal imagery and CamTrawl. Mar. Technol. Soc. J. **49**(2): 99–106. doi: 10.4031/MTSJ.49.2.10.

Stafford, K.M., Ferguson, M.C., Hauser, D.D.W., Okkonen, S.R., Berchok, C.L., Citta, J.J., Clarke, J.T., Garland, E.C., Jones, J., and Suydam, R.S. 2016. Beluga whales in the western Beaufort Sea: Current state of knowledge on timing, distribution, habitat use and environmental drivers. Deep Sea Res., Part II In press. doi: 10.1016/j.dsr2.2016.11.017.

Sweeney, K.L., Helker, V.T., Perryman, W.L., LeRoi, D.J., Fritz, L.W., Gelatt, T.S., and Angliss, R.P. 2016. Flying beneath the clouds at the edge of the world: Using a hexacopter to supplement surveys of Steller sea lions (*Eumetopias jubatus*) in Alaska. J. Unmanned Veh. Syst. **3**(3): 114–112. doi: 10.1139/juvs-2015-0010.

Taylor, J.K.D., Kenney, R.D., LeRoi, D.J., and Kraus, S.D. 2014. Automated vertical photography for detecting pelagic species in multitaxon aerial surveys. Mar. Technol. Soc. J. **48**(1): 36–48. doi: 10.4031/MTSJ.48.1.9.

Thomas, L., Buckland, S.T., Rexstad, E.A., Laake, J.L., Strindberg, S., Hedley, S.L., Bishop, J.R.B., Marques, T.A., and Burnham, K.P. 2010. Distance software: Design and analysis of distance sampling surveys for estimating population size. J. Appl. Ecol. **47**: 5–14. doi: 10.1111/j.1365-2664.2009.01737.x. PMID: 20383262.

Tweedie, M.C.K. 1984. An index which distinguishes between some important exponential families. *In* Statistics: Applications and new directions. Proceedings of the Indian Statistical Institute Golden Jubilee International Conference. *Edited by* J.K. Ghosh and J. Roy. Indian Statistical Institute, Calcutta, India. pp. 579–604.

Vas, E., Lescroël, A., Duriez, O., Boguszewski, G., and Grémillet, D. 2015. Approaching birds with drones: First experiments and ethical guidelines. Biol. Lett. **11**: 20140754. doi: 10.1098/rsbl.2014.0754. PMID: 25652220.

Vate Brattström, L., Mocklin, J., Tudor, B., George, J.C., and Givens, G.H. 2016. Update on the bowhead whale aerial photoID program and 2011 aerial spring survey. Presented to the 66th International Whaling Commission, Bled, Slovenia. Paper SC/66b/BRG/04.

Ver Hoef, J.M., and Boveng, P.L. 2007. Quasi-Poisson vs. negative binomial regression: How should we model overdispersed count data? Ecology, **88**(11): 2766–2772. doi: 10.1890/07-0043.1. PMID: 18051645.

Vermeulen, C., Lejeune, P., Lisein, J., Sawadogo, P., and Bouché, P. 2013. Unmanned aerial survey of elephants. PLoS ONE, **8**(2): e54700. doi: 10.1371/journal.pone.0054700. PMID: 23405088.

Watts, A.C., Perry, J.H., Smith, S.E., Burgess, M.A., Wilkinson, B.E., Szantoi, Z., Ifju, P.G., and Percival, H.F. 2010. Small unmanned aircraft systems for low-altitude aerial surveys. J. Wildl. Manage. **74**: 1614–1619. doi: 10.1111/j.1937-2817.2010.tb01292.x.

Wood, S.N. 2006. Generalized additive models: An introduction with R. Chapman and Hall/CRC, Boca Raton, Fla., USA. 391 pp.

Wood, S.N., Bravington, M.V., and Hedley, S.L. 2008. Soap film smoothing. J. R. Stat. Soc. Series B Stat. Methodol. **70**: 931–955. doi: 10.1111/j.1467-9868.2008.00665.x.